Proceedings Paper:
Chauhan, M orcid.org/0000-0001-9742-5352, Deshpande, N, Barresi, G et al. (4 more authors) (2017) Design and control of a novel robotic microsurgical forceps for Transoral Laser Microsurgery. In: 2017 IEEE International Conference on Advanced Intelligent Mechatronics (AIM). 2017 IEEE International Conference on Advanced Intelligent Mechatronics (AIM), 03-07 Jul 2017, Munich, Germany. IEEE , pp. 737-742. ISBN 978-1-5090-5998-0

https://doi.org/10.1109/aim.2017.8014105

Design and control of a novel robotic microsurgical forceps for Transoral Laser Microsurgery

Manish Chauhan[1], Nikhil Deshpande[1], Giacinto Barresi[1], Claudio Pacchierotti[2],
Domenico Prattichizzo[1], Darwin G. Caldwell[1], and Leonardo S. Mattos[1]
[1]Department of Advanced Robotics, Istituto Italiano di Tecnologia (IIT), Via Morego 30, Genova, 16163, Italy.
[2]CNRS at Irisa and Inria Rennes Bretagne Atlantique, Campus de Beaulieu, 35042 Rennes cedex, France.
Email: manish.chauhan@iit.it

***Abstract*—A master-slave configuration robotic microsurgical forceps is presented here which is capable of performing micro tissue manipulation. The master, i.e., 7 degree of freedom (DOF) haptic device (*Sigma.7*) tele-operates the slave device which is a combination of a 6-DOF serial robotic arm and a 1-DOF (open/close) forceps device. The serial robotic arm is used for positioning and orienting the robotic microsurgical forceps which is integrated with a force/torque sensor for tissue grip-force measurement. This integrated system is analyzed for its (i) functional performance, (ii) usability, and (iii) haptic performance through user trials. The new system offers improved tool placement, enhanced tissue perception, safety, and accuracy. The traditional manual forceps are therefore, replaced with an easy-to-use and ergonomic robot assisted device.**

***Index Terms*—Robotic minimal invasive surgery, microsurgical forceps, haptic interface, transoral laser microsurgery.**

I. Introduction

Transoral Laser Microsurgery (TLM) deals with treatment of malignancies in the laryngeal region for malignancies such as cysts, polyps, nodules, carcinoma. Treatment of these malignant tissues involve accessing the vocal cords (surgical site) through the larynx, which has the shape of an irregular closed cylinder. This shape offers a wide range of challenges to the surgeons for pathology removal. These challenges are broadly due to three factors, (i) **Surgical site**: The vocal cords are limited to 17-21mm for males and 11-15mm for females [1] which makes it difficult to access all its areas, (ii) **Surgical tools**: They offer one degree of freedom and are long (length $200-240mm$ exclusive of tool handle, diameter $2-2.5mm$) rigid structure tools, and (iii) **Surgeon interface**: The manual handling makes it unwieldy for surgeons to perform intraoperative task ergonomically.

Figure 1 shows the exposure method of the surgical site using a laryngoscope (approximate length of $180mm$ and cross-section $16 \times 23mm^2$) which is inserted through the mouth of the patient such that direct line-of-sight is established for the surgical microscope. A CO_2 laser beam is aimed at surgical site from a distance of $400mm$ with the help of a mechanical micro-manipulator joystick. The combination of the laryngoscope and micro-manipulator consumes a depth of $300-340mm$ out of the total $400mm$ working range. This leaves the surgeons with a narrow range of $50-60mm$ range for microsurgical tool movement and tissue manipulation. This poses a functional challenge for surgeons in order to access and resect in the different parts of the vocal folds [2]. The manual handling of the traditional tools is cumbersome, non-ergonomic and also induces hand tremors which negatively impact surgical outcome.

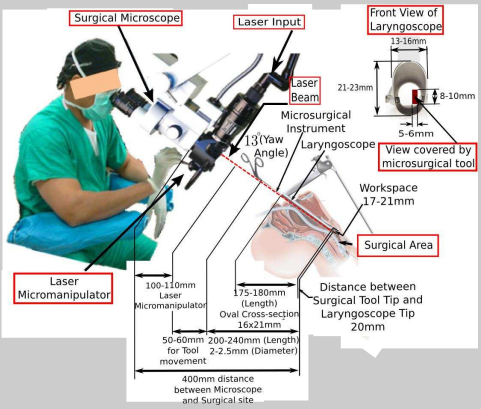

Fig. 1. Traditional constraints in TLM operating room

For best surgical results under above mentioned constraints, it would be beneficial to improve functionality and reach of these tools by adding automated robotic control. With a focus on improving the surgeon-machine interface, the research in this paper extends the benefits of robot-assisted technologies to the critical aspect of tissue manipulation in TLM and presents the design and development of a novel, robotic microsurgical forceps with the surgeon using an ergonomic interface with haptic feedback for improved surgical perception and task outcome. Earlier research in this context resulted in the design of a robot-assisted forceps device presented in [3]. However, in using the device in a realistic surgical scenario, key issues were identified related to the size of the device, which caused occlusion of the surgical site. The device presented in this paper focuses on resolving these issues and meeting the dimensional and operational constraints of TLM through the design of a next generation robotic forceps for enhancing the performance, accuracy & safety of the surgery.

II. Related Work

Various robot-assisted surgical tools have been developed by different groups over time. Snake-like manipulators with high tip dexterity for tissue manipulation and suturing [4] have been explored by Simaan et al. A cooperatively controlled bimanual teleoperation robot having 3-DOF wrists with surgical tools attached was developed by He et al. [5]. Wang et al. [6] presented a new robot-assisted master-slave laryngeal surgery system consisting of two symmetrical 9-DOF manipulators, with quick-change interfaces for surgical tools. Rivera-Serrano et al. [7] presented a highly articulated robot in a follow-the-leader mechanism using a master controller. Solares and Strome [8] and Desai et al. [9] have explored the utility of the *da Vinci Surgical System* [10] for TLM but found size of the *da Vinci* tool shafts as a major limitation along with constant change of attendant during surgery. An effective solution was presented by Maier et al. [11] where standard surgical tools could be attached to a lightweight manipulator without any modification. Despite extensive research efforts, these instruments are not particularly focused in assisting the TLM application. New robotic instruments are needed for this specific and challenging microsurgical application.

To enhance surgeon performance, along with providing robot assisted teleoperation, haptic feedback is also important for enhanced intra-operative perception accuracy [12]. These benefits lend themselves readily towards facilitating and improving the complex suite of otolaryngological techniques of tool control involved in TLM. Having understood these challenges, it is important to create a device which addresses them with the benefits of teleoperated surgery and haptic perception.

III. Robot-assisted Microsurgical Forceps Design

With reference to the discussion in sec. I, the motivation of the design was to build a standalone motorized microsurgical forceps which improves motion accuracy, reduces the dependence on operator dexterity, and facilitates easy tissue manipulation and surgical exposure, all the while satisfying the design constraints as noted in Fig. 1. The key design specifications of these components are based on the constraints offered by TLM which are listed in Table I. The novel design consists of three modules: (i) the tool shaft; (ii) the tool actuation mechanism; and (iii) the tool-shaft holder.

A. The tool shaft

This component is a modified version of the traditional microsurgical tool shaft, made up of an outer shaft (ϕ $2mm$) which holds an inner translating wire (*itw*,ϕ $1mm$). The translation of this wire (motion of about $3mm$) provides the open-close DOF of the tool jaw. The tool shafts are of two types: (i) where pushing action of the *itw* closes the tool jaws, and (ii) where pulling action of the *itw* closes the jaws. One adaptation is introduced at the proximal end of the tool shaft with a short hollow tube with $M3$ internal threading. This adaptation acts as a docking interface for the tool shaft with the "tool-shaft holder" (Refer Fig. 2(a)).

TABLE I
Design specifications of the microsurgical forceps

Design Limits	Remarks
Tool maneuverability range of 70-80mm.	In order to be operable under the surgical microscope.
Displacement from microscope line-of-sight of 200mm.	In order to avoid interference and maintain distance between the tool base and laryngoscope entry point.
Tool footprint under microscope of 5mm.	In order to maintain minimum vision occlusion when viewed through the microscope.

B. Tool actuation mechanism

The tool actuation mechanism consists of a set of five linkages ("L1","L2", "L3", "L4", "L5"), which are designed to provide linear translation of the *itw* through kinematic inversion. Here, the link "L1" is treated as ground, i.e., the hinge link. Link "L2" forms the input link (i.e., slider) along the *"actuator axis"*. Link "L2" transfers direct motion to link "L3" which in-turn transfers motion to link "L4" through the ground/hinge link "L1". Links "L3" and "L4" have an inverse relationship. Link "L4" is directly coupled with link "L5". Link "L5" (i.e., wire pusher) is connected to and actuates the *itw* of the tool shaft along the "*tool axis*" (Refer Fig. 2(b)). A force sensor (ATI Nano17) is located with its measurement axis coincident with the *"actuator axis"* of link "L2" optimally for allowing the sensing of the tissue gripping force. The closing of the gripper jaws (along *"tool axis"*) on tissue transmits a reaction force on to the surface of the sensor through the link "L2" (along *"actuator axis"*). The force sensor, attached to link "L2", outputs a signal in direct proportion to the tissue gripping force.

C. Tool-shaft holder

Figure 2(c) shows the design of the tool-shaft holder which connects the tool shaft with tool actuation mechanism. The tool shaft holder frame comprises of three sub-frames "F1", "F2", and "F3". The tool shaft itself is attached rigidly to sub-frame "F1" at point "P1" such that the "*tool axis*" is at an offset of $200mm$ from the *"actuator axis"*. The cross-sectional thickness of "F1" is designed to be $5mm$. Both these aspects are in keeping with the constraints listed earlier. Further, the sub-frames "F1" and "F2" are rigidly connected at "P2" (i.e. *"support axis"*). The sub frame "F3" is designed as an attachment bracket. A linear actuator (Nanotec L2018 series) placed on "F3" drives the open/close DOF through these set of linkages.

IV. The novel straight-line mechanism and its validation with ADAMS simulation

The tool open/close DOF is actuated by a mechanism which is designed as a graphical synthesis method in two-stages. This five-link mechanism is synthesized as a Function

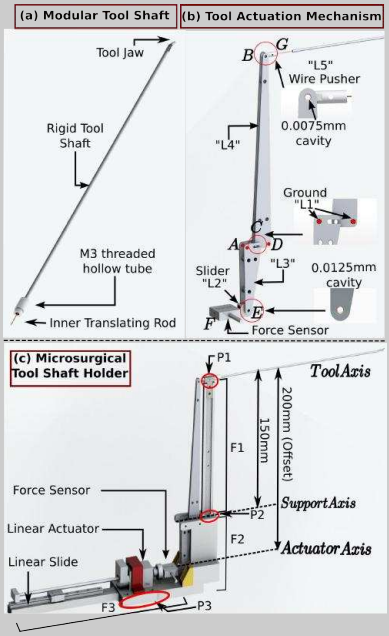

Fig. 2. Robot assisted Microsurgical forceps design

Generator [13] problem (where output motion is linearly related to input actuation) to provide straight line motion of the *itw*.

1) In the first stage of synthesis, a suitable three link mechanism is formed which can allow linear displacement of the slider (i.e., link "L2": F-E) within limits $(x_i,\ x_f)$ along the *"actuator axis"*. Here x_i and x_f are the initial and final positions of slider motion, i.e., 0 and $3mm$ respectively. The kinematic synthesis begins with an arbitrary choice of hinge point A at an offset of $50mm$ from the *"actuator axis"* in Y-direction. (Refer Fig. 3). On the *"support axis"* another point C is chosen at a distance of $10mm$ from point A in X-direction. The end point E of link "L2" is chosen on the *"actuator axis"* such that its position lies on the vertical line passing through point A. Joining the three points $A-C-E$, a triangular shaped link is achieved, named as "L3". The linear displacement of link "L2" causes link "L3" to translate in angular motion (θ_i, θ_f). To ensure that the link "L2" follows a straight-line trajectory between x_i and x_f, three additional intermediate Chebyshev's precision points[14] are chosen using the equation 1.

$$x_j = a - hcos[(2j-1)\cdot\pi/2n] \qquad j = 1,\ 2,\ 3 \quad (1)$$

The variables a and h are defined as $(x_i + x_f)/2$ and $(x_f - x_i)/2$ respectively. The choice of three Chebyshev's precision points (n) is deemed sufficient for the design to allow the slider to follow an exact straight line path. The three precision points are $x_1 = 0.2mm$, $x_2 = 1.5mm$ and $x_3 = 2.799mm$. The link "L2" starts from x_i passes through the three precision point x_1, x_2, x_3 & finishes its stroke at its final position x_f. Since link "L2" is rigid, points F and E have identical movement. This displacement of link "L2" causes angular motion of link "L3" through corresponding positions $(\theta_i, \theta_1,\ \theta_2,\ \theta_3,\ \theta_f)$. A closer observation of link "L3" $(A - C - E)$ shows that a displacement of $1mm$ of end point E in X direction (Fig. 4(a)) causes its simultaneous displacement of $0.0130mm$ in Y direction (Refer Fig. 4(b)). This small Y displacement is because of angular motion of link "L3" with reference to the hinge point A. Though this displacement is negligible, a small cavity is introduced in link "L3" at end point E to ensure that link "L2" translates in X direction only.

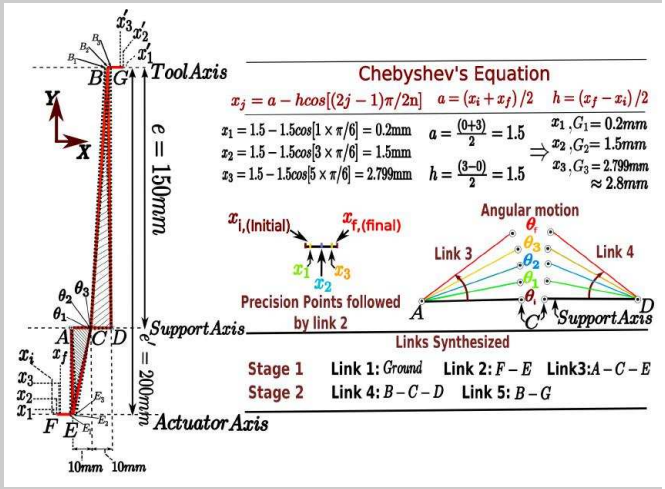

Fig. 3. Kinematic Synthesis of Mechanism for surgical tool actuation

2) In the second stage of synthesis, two links are fabricated such that the motion from *"actuator axis"* can be transferred to *"tool axis"*. First, a hinge point D is chosen along *"support axis"* at a distance of $10mm$ from point C in X- direction. Another point B is assumed on the *"tool axis"* which is at a distance of $150mm$ from *"support axis"* in Y-direction. The triangular link $B - C - D$ so created is termed as link "L4". Point C serves as the common engagement point for links "L3" and "L4". This implies that the angular motion of link "L3" through $(\theta_i, \theta_1,\ \theta_2,\ \theta_3,\ \theta_f)$ is mirrored by link "L4" at point C. Finally, the last link in this synthesis is assumed to be connected at the end point B , link $B - G$ or "L5". The angular motion of link "L4" is transferred to the *wire-pusher* link "L5" such that it produces the corresponding straight line translation of the *itw*. The precision points for link "L5" are $x_1^{'}$, $x_2^{'}$, $x_3^{'}$. The ratio of the link lengths "L4" and "L3" results in a *link-ratio* of 3. With this arrangement, a displacement of $1mm$ at end point E results in a displacement of $3mm$ at end point B which is sufficient to produce the relevant open/close of the forceps jaws. The displacement of $150mm$ for link "L4" allows

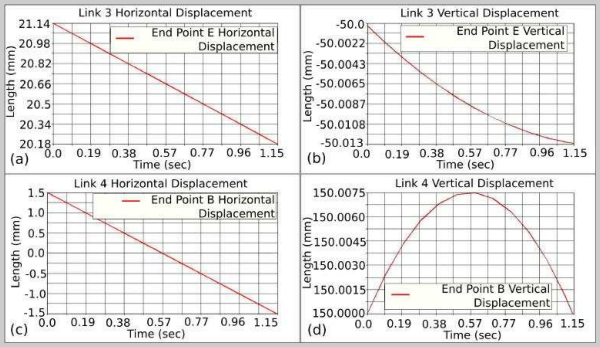

Fig. 4. Curvi-linear motion of Link 3 and 4

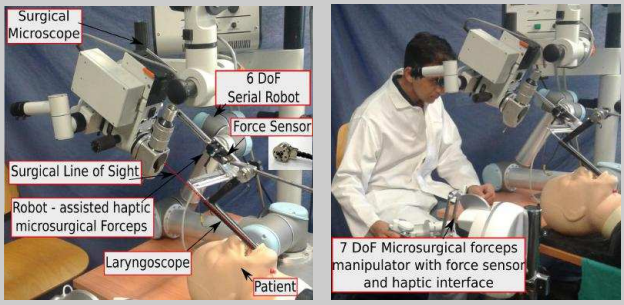

(a) Closeup view under surgical microscope (b) Haptic feedback integration

Fig. 5. Microsurgical forceps integration control by Master slave configuration

minimum vision occlusion under surgical microscope and reduced interference with other surgical setup. As was evident for point *E* of link "L3", here too, the angular motion of point *B* causes a simultaneous *X* and *Y* displacement. Figure 4(d) shows the displacement of $0.0075mm$ in Y direction. Again, though this displacement is negligible, a cavity is provided in link "L4" at point *B* to permit only linear displacement of link "L5" (Refer Fig. 2(b)).

On performing the mobility analysis for the synthesized mechanism using the Grübler's criterion [15], it was found that the mechanism's motion DOFs were *two*. Here, the first DOF is the linear translation of link "L5" $(B-G)$ and the second DOF can be explained as the negligible motion in the Y direction for the end points E and B for links "L3" and "L4". In the present design, the second DOF is neglected as only one DOF motion is needed (i.e., forceps jaw open/close). Finally, the angular movements of links "L3" and "L4" are possible in both clockwise and anticlockwise direction which makes the design adaptable for both the types of microsurgical forceps as discussed in sec. III-A.

V. Integration and Control of Robot Assisted Device with Serial Manipulator

In continuation with the discussion in sec. III-C, the above designed device was integrated with a 6 DOF Univeral Robot serial manipulator (UR5 [16]) in order to position the tool exactly at the surgical site. Hence, the Denavit-Hartenberg parameters for the robot[1] were suitably updated to operate as a 7-DOF manipulator (6-DOF serial + 1 DOF open/close). Figure 5(a) and (b) shows the integration of this device which is controlled through teleoperation by a 7 DOF haptic master (Force Dimension *Sigma.7* [17]).

A. Control and haptic feedback Design

Linux-based software was written using the open-source Robot Operating System (ROS) platform for controlling the 7-DOF manipulator. The velocities of the robotic manipulator joints $\dot{q} \in \mathbb{R}^6$ can be expressed as:

[1]http://rsewiki.elektro.dtu.dk/index.php/UR5

$$\dot{\mathbf{q}}_\mathbf{r} = \mathbf{J}^{-1}\dot{\mathbf{q}}_\mathbf{h}\zeta \tag{2}$$

where $\mathbf{J}^{-1}$ is the Moore-Penrose pseudo-inverse of the manipulator Jacobian matrix $\mathbf{J} \in \mathbb{R}^{7x6}$ and $\dot{\mathbf{q}}_\mathbf{h} \in \mathbb{R}^7$ are the velocities of the *Sigma.7*'s end-effector. The gesture scaling factor ζ is tunable to allow coarse and fine gestures in different stages of operation. For the purposes of this research, the velocity of the 7^{th}-DOF (gripper) of the haptic master is considered zero. The $\dot{\mathbf{q}}_\mathbf{h}$ velocities of the master end-effector are scaled through a low-pass filter in equation (3), with a tunable factor β to control the level of high-frequency tremor suppression.

$$\dot{\mathbf{q}}_\mathbf{h}^k = (1-\beta)\cdot\dot{\mathbf{q}}_\mathbf{h}^{k-1} + \beta\cdot\dot{\mathbf{q}}_\mathbf{h}^{encoder} \tag{3}$$

Sigma.7's gripper DOF were mapped directly to the open/close DOF of the microsurgical forceps such that while a tissue is gripped with this forceps, the sensed value from the ATI sensor is filtered using a low-pass filter and then scaled for rendering to the 7^{th} (gripper) DOF of the *Sigma.7*. The following equations are used.

$$\begin{aligned} f_g^k &= (1-\beta)\cdot f_g^{k-1} + \beta\cdot f_g^{sensor} \\ f_g^{omega} &= \kappa\cdot f_g^k \end{aligned} \tag{4}$$

The values used for the constants are: $\beta = 0.001$ and $\kappa = 4$. The haptic rendering loop is run at 500 Hz.

VI. Evaluation & User Trials

In order to establish (i) the tool's motion and gripping performance; (ii) the usability of the device, including the haptic master interface; and (iii) the utility of the gripping force haptic feedback, user trials were conducted with the integrated device where different subjects operated the haptic master interface in a ring-to-peg transfer task (Refer inset, Fig. 6). This task was chosen due to its similarity in nature to the general surgical tasks like gripping and pulling a tissue out of the larynx. The experiments were conducted under two conditions: (i) C1: with haptic feedback; and (ii) C2: without haptic feedback. 12 subjects were chosen for the comparative analysis between the two conditions.

The subjects were divided into two sets of 6 each. "Set A" performed trials in two separate sessions, in the sequence C2-before-C1, while "Set B" did the trials in the sessions of C1-before-C2. This was done to avoid subjective bias in the results coming from the order of presentation of the haptic condition.

Each subject performed a set of 6 trials under both the conditions in order to account for the learning aspects. For uniform results, the UR5 robot was programmed to start from the same home position at the beginning of each trial. During each trial the following measurements were made, (i) Time required to pick-up the O-ring from a peg, (ii) Total time required to pick-n-place the O-ring from one peg to the other, (iii) Number of attempts made to pick up the O-ring from a peg, (iv) Number of ring drops in between pick-n-place of the ring, (v) the Trajectory executed for the task, and (vi) the Measurement of the applied gripping force on the O-ring surface for both the C1 and C2 conditions (only for Set B).

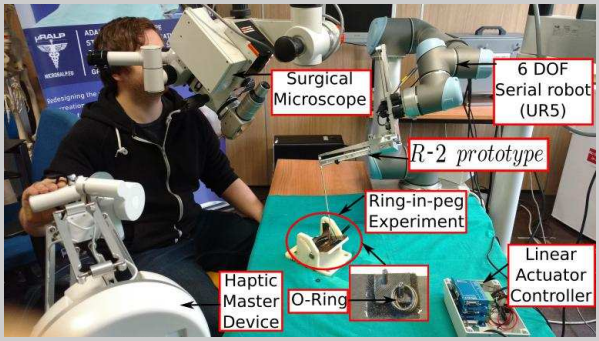

Fig. 6. Ring-in-peg experiment with $R-2$ prototype

TABLE II
EVALUATION STATEMENTS

S1. The control of the device was precise.
S2. The control of the device induced fatigue in my hand.
S3. I had to work hard to accomplish the task with this device.
S4. The control/use of the device was easy.
S5. I found the device was easy to learn, so I could start using it quickly.
S6. I was stressed, irritated, and annoyed using this device during the task.
S7. I would like to use this device again for this kind of task.
S8. My performance in this task with this device was satisfying
S9. It was easy to make errors with this device.
CP. Preference of condition 1 or condition 2

(Age of subjects. Mean=27.75 years with SD=2.95 years. Gender. 9 Male, 3 Female)

A subject-wise experience evaluation was collected through a questionnaire made of 9 statements describing different aspects of tool performance and user experience (Refer Table II). The subjects had to indicate their degree of agreement with each statement along a line divided in 7-point Likert-type scale [18] (the score "1" means "I strongly disagree", while "7" implies "I strongly agree") which was presented to them after trials in each of the conditions. At the end of the second presented condition, the subjects also had to compare their overall experience with both conditions by expressing a degree of condition preference (CP) for C1 or C2. Based on all the above measurements and subjective evaluations, it was intended to conduct three major analyses at the end of this experiment: (i) Performance analysis of the device; (ii) Usability of the device; and (iii) the Haptic performance analysis.

A. Device Performance Analysis

Two aspects were considered here: (i) the trajectory analysis for the trials; and (ii) the time taken by the subjects in conducting the tasks.

1) Trajectory Analysis : Change in trajectory lengths (improvement or deterioration) over the trials performed by the subjects was chosen as a metric for making a comparison among subjects in order to establish the device performance. Since each subject performed 6 trials, the ratio of the lengths of the subsequent 5 trials was calculated against the first trial. It was found that the ratio of the last $\left(6^{th}\right)$ trial was **0.8273**, while the average ratio over the 5 trials was **0.9218**. Both values being less than 1 demonstrates a positive performance for the device.

2) Execution Time Analysis: The overall time for task completion is also a good metric for device's performance evaluation. Hence, (i) time to lift the ring from the peg (T_{lift}); and (ii) time to transfer the ring from peg-to-peg (T_{total}) were analyzed in the experiment. It was observed (Refer Fig. 7) that T_{lift} reduced from 72.17 seconds to 42.25 seconds over the 6 trials with an improvement of 41%. The same trend for T_{total} was obtained where it went from 94.4 seconds to 56.8 seconds, giving an improvement of almost 40% here as well. This demonstrated that the device allows a fast learning curve.

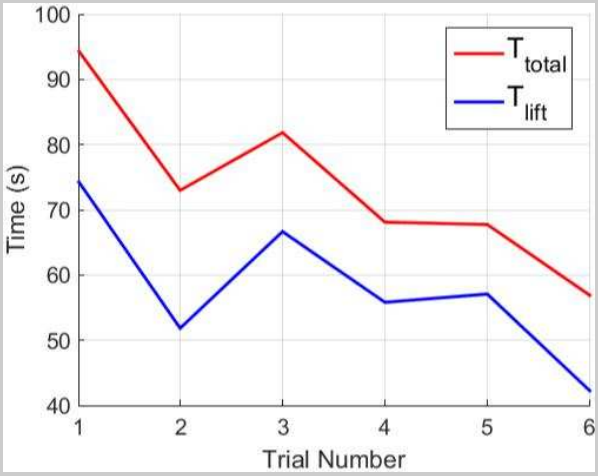

Fig. 7. Comparison of average time over trials

B. System Usability Analysis

Two aspects were evaluated: (i) user subjective evaluation of device accuracy; and (ii) the ease-of-use and effort while using the device.

1) User Accuracy evaluation: This metric gives an indication of the perception of the users with respect to the device's accuracy and performance. As seen from overall scores in Table III (statements S1, S7, S8, and S9), all the values are greater than 4 on a 7-point Likert-type scale, indicating a positive evaluation of the device. For S1, the users evaluate the device at (**5.455 / 7**), giving high marks for its precision in the tasks. This aspect is also confirmed by S8 where the subjects are comfortable and satisfied with their performance using the device (**5.33 / 7**).

TABLE III
SCORES FOR QUESTIONNAIRE

	Subject Trials				
	C1		C2		Overall Scores
	m	sd	m	sd	m
S1	5.58	0.64	5.33	1.59	5.455
S2	3.00	1.73	2.41	0.86	2.705
S3	3.91	1.49	3.16	1.46	3.535
S4	4.91	1.11	4.58	1.65	4.745
S5	5.75	1.16	5.5	1.44	5.625
S6	2.25	1.23	2.66	1.02	2.451
S7	5.25	1.42	5.16	1.28	5.205
S8	4.91	1.55	5.75	1.16	5.33
S9	4.08	1.38	3.91	1.60	3.995
CP	m=4.08; sd = 2.09				

2) Usability Analysis: The overall scores for remaining statements S2, S3, S4, S5, and S6 pertain to the overall usability, ergonomics, and usage fatigue. Low values on S2 and S6 indicate that the device does not demand high mental effort from the subjects, while the high scores on S4 and S5 show that the device is easy to use and learn quickly. The middling score on S3 (**3.535 / 7**) relates to the informal feedback from the subjects where they demanded additional DOF in the forceps for easier alignment with the O-ring.

C. Haptic Performance Analysis

A comparative analysis of the device in the C1 and C2 conditions is done for both set of subjects with respect to: (i) the Trajectory performance, (ii) Time analysis, (iii) the Force feedback performance, and (iv) the subjective evaluation using the questionnaire.

1) Trajectory Analysis of robot: It was found that the overall trajectory ratio in C1 was much lower than that for C2 condition. Also, it was seen that irrespective of the order of presentation of the device, the average ratio of robot trajectory was smaller in C1 (**Set A** (C1:0.77, C2:0.9654) and **Set B** (C1: 0.8926, C2: 1.0592)). Though this value is not significantly smaller, it indicates a trend where haptic feedback prompts better performance with the robot.

2) Time analysis for task performance::

1) Time required for lifting the ring: There was no significant difference between time response for each subject to lift a ring from a peg in both conditions with mean time of 55.7s for C1 and 57.8s for C2. But a comparison of the number of attempts done to lift the ring from a peg (errors) shows that the condition C1 is unfavorable (with 22 occurrences) with respect to C2 (with 18 occurrences).
2) Time required for pick-n-place of the ring: Similarly, no significant difference was seen in comparison of time response for picking up the ring from a peg and placing it in the other for both conditions (mean time of 71.8s for C1 and 73.5s for C2). But a comparison of total number of ring drops (errors) after lifting it shows that the condition C1 is unfavorable (with 5 occurrences) with respect to C2 (with 3 occurrences).

3) Gripping force analysis: Force application by subjects while gripping the O-rings was analyzed for establishing the tool capability during teleoperation. Figure 8 shows this comparison with a box plot under conditions C1 and C2 for subjects in **Set B**. It can seen that the gripping force applied under condition C1 is significantly less in comparison to condition C2 indicating an awareness of the force required to grasp the ring in condition C1, which was not the case in C2.

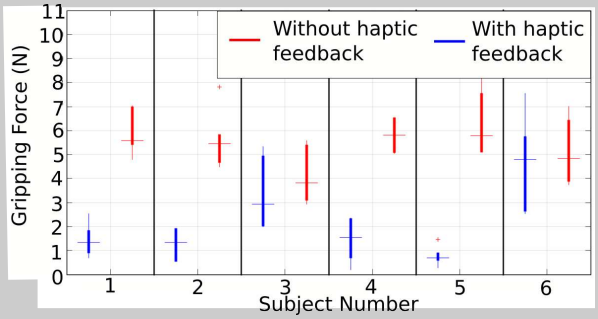

Fig. 8. Subject-wise comparison of gripping force

In order to get a better perception while gripping with forceps, a comparison of average gripping force applied by subjects was made. It was found that the mean force applied on the ring was less in condition C1 (p = 7.4189e-04) according to *student's t-test* with respect to condition C2 (2.158N vs 5.606N). This result indicates that gripping force feedback can allow enhanced perception as well as safety, limiting the force applied for tissue gripping. This result agrees with the conclusion in [19], where the mean applied force was less under haptic feedback condition.

4) Subjective evaluation with questionnaire: The scores for the questionnaire in Table II were evaluated to understand the effect of gripping force feedback on task completion time through Friedman test [20], whose results are listed in the Table III. It can be seen from statements S1, S2, S4, S5, S6 and S7 that the subjects were not able to judge the performance of device with respect to the two conditions. In Table III, the performance parameters of robot assisted device control, its learning and induction of fatigue got higher scores in condition C1. But this score had no significant difference with respect to the corresponding one's in condition C2. These results confirm with the comparison drawn earlier where the time required to perform the experimental task was

not significantly different. Also, it can be seen on comparing the scores of statement S3, S8 and S9 that the performance of device suffered marginally in context of errors occurring in condition C1. This also complies with the results where higher number of errors were committed during condition C1.

VII. Discussions

Based on the above discussion, it can be summarized that the performance of the new robotic device was significantly better in context of gripping force applied on the ring and marginally better in context of time required to perform the task in condition C1. This was also confirmed by subject-wise evaluation in some of the statements. But the higher number of errors occurring during haptic condition led to a mixed feedback for the device. These contrasting results can be explained with the following reasons:

- The test was performed with the use of rubber O-rings whose surface is difficult to penetrate through unless high pinching force is applied. This tough surface rings were not allowing the force sensor to provide a reasonable force feedback at the master device. Due to this, not much statistical difference was found in the results from the two conditions, for the subjective evaluation.
- Subjects regulated the force applied in C1 while gripping the O-ring. This takes more attempts and requires training, thus induced more errors [19].

But as already mentioned, there was preference for condition 1 over condition 2. This indicated that with more realistic softer materials, better results could be achieved with force feedback.

VIII. Conclusion and Future Work

This paper presents a novel design of an integrated robot-assisted microsurgical forceps tool for intraoperative use in TLM. The new design complies with the TLM constraints and replaces the traditional manually operated tools with a teleoperation system consisting of: (i) an integrated 7 DOF microsurgical forceps; (ii) a 7-DOF teleoperation haptic master interface; and (iii) an integrated force/torque sensor for haptic feedback of the tissue gripping force. A comparative performance analysis of the device was done through user trials under with and without haptic force feedback which resulted in preference of force feedback condition. The system provides: (i) improved controllability and safety; (ii) reduced task completion time; (iii) enhanced surgical site perception with grip-force feedback; and (iv) intuitive and ergonomic operation of the microsurgical forceps with a common surgeon interface providing gesture scaling and overcoming the problems of hand tremors and wrist excursions.

In the extension of this research, an attempt to increase the tool workspace shall be investigated by addition of rotational DOF to tool shaft. This improved robotic tool shall be tested in collaboration with expert surgeons through ex-vivo and cadaver to validate the new technology in terms of surgical usability and safety.

References

[1] M. Hirano, "Morphological Structure of the Vocal Cord as a Vibrator and its Variations," *Folia Phoniatrica et Logopaedica*, vol. 26, pp. 89–94, 1974.

[2] P. A. Liverneaux, S. H. Berner, M. S. Bednar, S. J. Parekattil, G. M. Ruggiero, and J. C. Selber, *Telemicrosurgery: robot assisted microsurgery*. Springer Science & Business Media, 2012.

[3] N. Deshpande, M. Chauhan, C. Pacchierotti, D. Prattichizzo, D. G. Caldwell, and L. S. Mattos, "Robot-assisted microsurgical forceps with haptic feedback for transoral laser microsurgery," in *Engineering in Medicine and Biology Society (EMBC), 2016 IEEE 38th Annual International Conference of the*. IEEE, 2016, pp. 5156–5159.

[4] N. Simaan, R. Taylor, and P. Flint, "A Dexterous System for Laryngeal Surgery," in *Proc. Intl. Conf. on Robotics and Automation, (ICRA 2004)*, 2004, pp. 351–357.

[5] C. He, K. Olds, I. Iordachita, and R. Taylor, "A New ENT Microsurgery Robot: Error Analysis and Implementation," in *Proc. Intl. Conf. on Robotics and Automation, (ICRA 2013)*, 2013, pp. 1221–1227.

[6] S. Wang, Q. Li, J. Ding, and Z. Zhang, "Kinematic Design for Robot-assisted Laryngeal Surgery Systems," in *Proc. IEEE/RSJ Intl. Conf. on Intelligent Robots and Systems (IROS 2006)*, 2006, pp. 2864–2869.

[7] C. M. Rivera-Serrano, P. Johnson, B. Zubiate, R. Kuenzler, H. Choset, M. A. Zenati, S. Tully, and U. Duvvuri, "A Transoral highly flexible robot: Novel technology and application," *The Laryngoscope*, vol. 122, no. 5, pp. 1067–71, 2012.

[8] C. A. Solares and M. Strome, "Transoral Robot-assisted CO_2 Laser Supraglottic Laryngectomy: Experimental and Clinical Data," *The Laryngoscope*, vol. 117, no. 5, pp. 817–820, May 2007.

[9] S. C. Desai, C. K. Sung, D. W. Jang, and E. M. Genden, "Transoral Robotic Surgery using a Carbon-dioxide Flexible Laser for Tumors of the Upper Aerodigestive Tract," *The Laryngoscope*, vol. 118, no. 12, pp. 2187–2189, Dec. 2008.

[10] da Vinci Surgical System. Intuitive Surgical Inc. CA, USA. Accessed on 6-Sept-2013. [Online]. Available: www.intuitivesurgical.com

[11] T. Maier, G. Strauss, M. Hofer, T. Kraus, A. Runge, R. Stenzel, J. Gumprecht, T. Berger, A. Dietz, and T. C. Lueth, "A New Micromanipulator System for Middle-Ear Surgery," in *Proc. Intl. Conf. on Robotics and Automation, (ICRA 2010)*, 2010, pp. 1568–1573.

[12] A. M. Okamura, "Methods for haptic feedback in teleoperated robot-assisted surgery," *Industrial Robot: An International Journal*, vol. 31, no. 6, pp. 499–508, 2004.

[13] C. H. Suh and C. W. Radcliffe, *Kinematics and mechanisms design*. Wiley, 1978.

[14] E. C. Kinzel, J. P. Schmiedeler, and G. R. Pennock, "Function generation with finitely separated precision points using geometric constraint programming," *Journal of Mechanical Design*, vol. 129, no. 11, pp. 1185–1190, 2007.

[15] G. Gogu, "Chebychev–grubler–kutzbach's criterion for mobility calculation of multi-loop mechanisms revisited via theory of linear transformations," *European Journal of Mechanics-A/Solids*, vol. 24, no. 3, pp. 427–441, 2005.

[16] Universal Robot 5. Universal Robots. Denmark. Accessed on 10-Feb-2016. [Online]. Available: http://www.universal-robots.com/products/ur5-robot/

[17] Force Dimension Omega.7. Force Dimension. Switzerland. Accessed on 10-Feb-2016. http://www.forcedimension.com/products/omega-7/overview. [Online]. Available: http://www.forcedimension.com/products/omega-7/overview

[18] J. G. Dawes, "Do data characteristics change according to the number of scale points used an experiment using 5 point, 7 point and 10 point scales," *International journal of market research*, vol. 51, no. 1, 2008.

[19] L. N. Verner and A. M. Okamura, "Effects of translational and gripping force feedback are decoupled in a 4-degree-of-freedom telemanipulator," in *Second Joint EuroHaptics Conference and Symposium on Haptic Interfaces for Virtual Environment and Teleoperator Systems (WHC'07)*. IEEE, 2007, pp. 286–291.

[20] E. Theodorsson-Norheim, "Friedman and quade tests: Basic computer program to perform nonparametric two-way analysis of variance and multiple comparisons on ranks of several related samples," *Computers in biology and medicine*, vol. 17, no. 2, pp. 85–99, 1987.